A Rapid Drift Modeling Method Based on Portable LiDAR Scanner

Zhao Huijun[1], Liu Chao[2], Qi Yunpu[3], Song Zhanglun[4], Xia Xu[5]
Norin Mining Limited, Beijing 100053, China[1, 2, 3, 4]
DIMINE Co., Ltd., Changsha 410083, China[5]

***Abstract*—Traditional measurement methods in underground mining tunnels have faced inefficiencies, limited accuracy, and operational challenges, consuming significant time and labor in complex environments. These limitations severely restrict the efficiency and quality of mine management and engineering design. To enhance the efficiency and accuracy of 3D modeling in underground tunnels, this study combines portable 3D LiDAR scanning technology with simultaneous localization and mapping. This integration enables autonomous positioning and efficient modeling without external positioning signals. The proposed approach effectively acquires high-resolution 3D data in complex environments, ensuring data accuracy and model reliability. High-resolution scanning of multiple critical areas was conducted on-site, with inertial navigation systems correcting the device's pose information. Automated data processing software was used for filtering, denoising, and modeling the collected data, leading to precise 3D tunnel models. Validation results indicate that portable laser scanning technology offers significant advantages in efficiency, accuracy, and safety, meeting the geological surveying and engineering needs of mining operations. The application of portable 3D laser scanning technology demonstrates considerable benefits in the rapid modeling of underground tunnels, providing effective technical support to improve mine management efficiency and safety. It also reveals broad application prospects.**

Keywords*—Underground mining; 3D modeling; portable 3D laser scanning; simultaneous localization and mapping (SLAM); mine surveying; inertial measurement unit (IMU)

I. Introduction

As mining resource development deepens, the scale and complexity of underground tunnel networks increase, raising higher demands for geological measurement and engineering management in mines[1], [2], [3]. High-precision 3D modeling forms the foundation of safe mining production and is crucial for optimizing engineering design and enhancing management efficiency [4], [5]. However, achieving efficient and accurate 3D modeling in the complex and harsh conditions of underground tunnels presents significant challenges.

Traditional surveying methods rely heavily on total stations and distance measuring devices. These methods often require manual point setting and observation, which are cumbersome and time-consuming, especially in poorly lit and dusty underground environments [6], [7]. Such conditions can compromise the efficiency and accuracy of data collection. Additionally, these methods depend significantly on the experience of survey personnel, making them prone to human error and limiting rapid responses to unexpected situations. Although static 3D laser scanning technology has significantly improved measurement accuracy, its application in underground spaces remains constrained by the complexity of equipment setup and positioning, which reduces flexibility and efficiency.

Recent advancements in 3D laser scanning technology, particularly the emergence of portable laser scanning devices, have provided an efficient and flexible solution for 3D modeling in complex environments. These portable devices utilize a non-contact measurement approach, enabling the rapid acquisition of high-resolution point cloud data. When combined with simultaneous localization and mapping (SLAM) technology, these devices achieve autonomous positioning and mapping in GPS-denied environments. Due to these technical advantages, portable laser scanning devices have increasingly been applied in fields such as construction [8], [9], [10], geological exploration [11], [12], [13], and autonomous driving [14], [15], [16]. Despite such advancements, research and application in underground tunnel environments remain limited, necessitating further exploration of portable laser scanning technology in these settings.

In this context, this study proposes a technical solution for rapid modeling of underground mine tunnels by integrating portable 3D laser scanning devices with inertial measurement units (IMU). By combining SLAM algorithms with inertial data in complex underground environments, this approach addresses laser radar positioning error accumulation and generates high-precision 3D models through automated data processing. The objective of this study is to validate the feasibility of portable 3D laser scanning technology in underground tunnel modeling and evaluate its advantages in terms of efficiency, precision, and applicability. Through testing and analysis of actual mining projects, the performance of this technology is assessed, and its potential applications in mining management and engineering design are further explored. This research provides an effective technical pathway for efficient modeling of underground tunnels and contributes to advancing 3D modeling technology in complex environments.

The remainder of this paper is organized as follows: Section II reviews related works and identifies research gaps. Section III details the proposed methodology integrating portable LiDAR, SLAM, and IMU. Section IV presents experimental results from engineering applications. Section V discusses the findings and compares with existing methods. Finally, Section VI concludes the study and outlines future directions.

II. Related Work

In recent years, research on 3D modeling of mining tunnels has gained traction, focusing on the application of 3D laser scanning technology, point cloud data processing and analysis, and innovations in positioning and navigation technologies. Traditional surveying methods for mining tunnels often rely on total stations and distance measuring devices. However, these methods face challenges such as inadequate measurement accuracy, cumbersome operations, and high time costs. In contrast, 3D laser scanning technology enables the rapid acquisition of high-precision spatial information, making it the preferred method for mining tunnel measurement and modeling [17], [18], [19]. Particularly in complex underground environments, laser radar can obtain data non-contact, overcoming the limitations of traditional surveying methods.

The introduction of SLAM technology has significantly enhanced data collection accuracy and efficiency in mining tunnel 3D modeling [20], [21], [22]. By continuously updating the device's pose, SLAM avoids the reliance on external positioning signals, which are often unavailable in GPS-denied underground environments.

IMU have also played a crucial role in mining 3D modeling by providing real-time motion state information [23], [24]. This data is vital for improving the stability and accuracy of SLAM systems in dynamic environments.

Regarding point cloud data processing, extracting useful information from large-scale point cloud datasets and removing noise remains a significant challenge [25], [26], [27], [28]. Existing studies have addressed this through techniques such as point cloud filtering, registration, and down-sampling. Point cloud filtering eliminates noise points generated during scanning, thereby improving data quality. Point cloud registration aligns data collected from different perspectives or times to construct continuous and consistent 3D models.

Despite substantial progress in the field of mining tunnel 3D modeling, the integration of portable laser scanning technology with SLAM and IMU still faces challenges. It is crucial to further minimize positioning errors in confined and complex spaces and ensure system stability in harsh environments. The maturity of the technology and its widespread application in the field require further validation and optimization. In Table I, the limitations of existing 3D modeling methods are summarized.

TABLE I. Limitations of Existing 3D Modeling Methods

Method	*Accuracy*	*Efficiency*	*Positioning Dependency*	*Environmental Adaptability*
Total Station	Medium	Low	High	Poor (dusty/low-light)
Static LiDAR	High	Medium	Medium	Moderate
SLAM-only Systems	Medium	High	None	Good (limited in dynamics)

While prior studies have advanced SLAM and IMU integration, three key limitations persist: (1) Cumulative errors in SLAM-based systems under prolonged operation, (2) Inadequate sensor fusion strategies for dynamic underground conditions, and (3) Limited validation in large-scale mining networks. Our approach addresses these through tight LiDAR-IMU coupling with error compensation (Section III.D) and field validation in 2.3km tunnel networks (Section IV).

III. Rapid Tunnel Modeling

A. Portable 3D LiDAR Scanning

Portable 3D laser scanning devices are developed based on SLAM technology, as shown in Fig. 1. Initially proposed by Smith and Cheeseman in 1986 to address spatial uncertainty estimation, SLAM primarily solves navigation and localization issues in unknown environments. It determines the device's position and orientation by observing features such as corners and columns, incrementally constructing an environmental map based on positional changes. SLAM enables concurrent localization and mapping, making it particularly suitable for complex underground mining environments where GPS signals are unavailable.

Fig. 1. Portable 3D laser scanning device.

Portable 3D scanning devices perform rapid and continuous scanning of complex environments while in motion, automatically capturing accurate three-dimensional spatial information. Compared to traditional fixed surveying techniques, portable devices address frequent setup issues caused by laser line-of-sight limitations, significantly enhancing fieldwork efficiency. These devices reduce operator labor intensity and safety risks while enabling extensive continuous 3D scanning tasks in underground mines.

In underground mining applications, portable 3D laser scanning devices integrate SLAM technology for autonomous localization and mapping in environments without external positioning signals, ensuring high-precision surveying capabilities. Their compact, lightweight, and ergonomic designs make them easy to transport and operate in confined or complex environments. Additionally, the integration of complementary sensors such as gyroscopes, accelerometers, and GPS enhances the collection of positioning and orientation data, substantially improving scanning accuracy and data reliability. These devices are capable of scanning various underground features, including tunnels, voids, and chutes, supporting tasks such as dimension measurement, volume calculations, morphology analysis, over-excavation and under-excavation assessments, engineering

quantity estimations, surface area measurements, and extraction of 3D contours and tunnel profiles.

B. Spatial Calibration Methods

The working principle of a 3D laser scanning system relies on laser ranging technology, which measures the time difference between laser emission and reflection to calculate the distance to an object's surface. By emitting a laser beam toward the object and receiving its reflected signal, the scanner determines the distance d based on the time-of-flight formula, as shown in Eq. (1).

$$d = \frac{c \cdot \Delta t}{2} \tag{1}$$

Where, c is the speed of light, and Δt is the time difference between the emission and reception of the laser.

To determine the three-dimensional coordinates of points on the object's surface, it is essential to measure not only the distance but also the emission angles of the laser beam. The laser scanner is typically mounted on a rotating device, allowing the laser beam to cover the entire scanning area through rotation. The three-dimensional coordinates (x, y, z) of each laser point can be calculated using the measured pitch angle θ, yaw angle ϕ, and the measured distance d, as shown in Eq. (2).

$$\begin{cases} x = d \cdot \cos(\theta) \cdot \cos(\phi) \\ y = d \cdot \cos(\theta) \cdot \sin(\phi) \\ z = d \cdot \sin(\theta) \end{cases} \tag{2}$$

Where, θ is the pitch angle of the laser beam, and ϕ is the yaw angle.

In practical applications, the laser scanner may move or rotate, necessitating consideration of its spatial position and orientation. Assuming the position of the scanner in space is PP and its rotation matrix is R, the three-dimensional coordinates (X, Y, Z) of the object's surface can be corrected using Eq. (3).

$$\begin{pmatrix} X \\ Y \\ Z \end{pmatrix} = R \cdot \begin{pmatrix} x \\ y \\ z \end{pmatrix} + \begin{pmatrix} x_0 \\ y_0 \\ z_0 \end{pmatrix} \tag{3}$$

Where, R is the rotation matrix.

By repeatedly performing this process, the scanner can calculate the three-dimensional coordinates of each laser point, thereby constructing the complete 3D point cloud data of the object or scene.

C. Mobile Scanning Method

The mobile scanning method uses highly integrated portable 3D laser scanning equipment to collect environmental data and generate 3D point cloud models during movement. The structure of the mobile scanning device, shown in Fig. 2, comprises a probe and a backpack. These components are interconnected via various communication protocols, including Ethernet, RS-485, RS-232, and GPIO control.

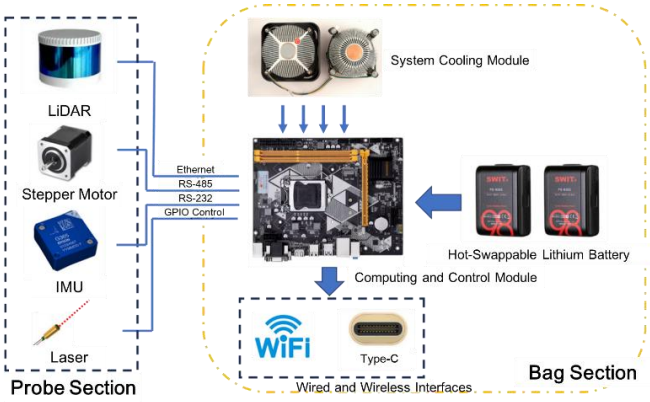

Fig. 2. Mobile scanning device structure.

The probe includes a LiDAR, stepper motor, inertial navigation module, and laser rangefinder, responsible for generating high-precision 3D point cloud data. The LiDAR measures the distance and shape of target objects, the stepper motor controls the scanning angle and rotation, the inertial navigation module provides device orientation information, and the laser rangefinder is used for accurate distance measurement.

The backpack focuses on performance and portability, containing a system cooling module, hot-swappable lithium battery, high-performance computing and control module, as well as wireless and wired interfaces. The cooling module ensures the stability of long-term device operation, the lithium battery provides continuous power, and the high-performance computing and control module processes data in real-time to generate precise point cloud models. The wireless and wired interfaces facilitate data transmission and device communication, supporting remote monitoring and data synchronization.

The mobile scanning process is illustrated in Fig. 3 and consists of four main steps:

1) Initial scanning and point cloud acquisition: Activate the LiDAR and scan the surrounding 3D space with the probe to capture the initial point cloud dataset, denoted as P_0.

2) Mobile remeasurement and data update: After the probe moves, use the LiDAR to rescan the previous area, obtaining the updated point cloud data denoted as P_1. This process continues to acquire new datasets P_2, P_3, and so on.

3) Trajectory estimation and spatial reconstruction: By comparing the two consecutive point cloud datasets P_t and P_{t+1}, estimate the probe's displacement and rotation by minimizing $T_{t \to t+1} = \arg\min_T \sum \left\| P_i^{t+1} - T \cdot P_i^t \right\|^2$, where T is the transformation matrix. The SLAM pipeline utilizes a feature-based Iterative Closest Point (ICP) algorithm that starts with feature extraction, where edge features (tunnel ribs) and planar features (tunnel walls) are extracted using curvature thresholds (edge: curvature > 0.1; planar: curvature < 0.05). Following this, dynamic object removal is performed through statistical outlier removal (50-neighbor points, 1.5 σ threshold) and DBSCAN clustering (ε=0.3m, minPts=15).

4) Point cloud registration and data fusion: Utilize the ICP algorithm to accurately align and fuse datasets $P_0, P_1, \ldots, P_t$, resulting in the creation of a continuous point cloud model M. Fine registration minimizes point-to-plane residuals using Huber loss with a threshold of δ=0.2m, expressed as $E = \sum \left| n_j^T (Rp_i + t - q_j) \right|^2$, where n_j represents the normal vector of the target plane j.

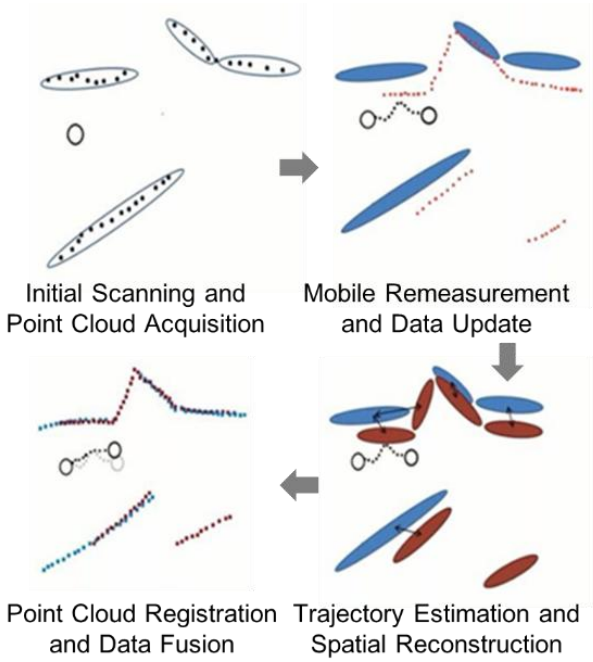

Fig. 3. Mobile scanning process.

D. Inertial State Integration

To mitigate positioning errors and inaccuracies caused by dynamic motion, an IMU is integrated into the system for spatial calibration. Traditional LiDAR systems often require stable platforms, but portable devices operating in dynamic environments can encounter vibrations and irregular movements that impact data accuracy. The IMU enhances measurement robustness by providing supplementary pose data.

The LiDAR is mounted on a linkage mechanism with dual rotational axes, as shown in Fig. 4. This configuration enables continuous acquisition of both laser ranging and inertial data, providing real-time six degrees of freedom (6DOF) trajectory estimation.

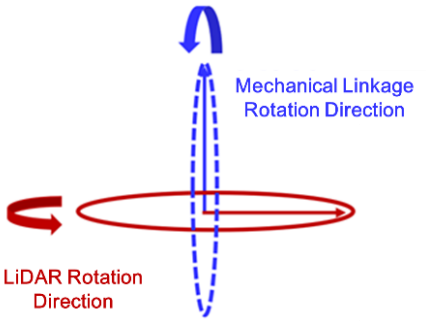

Fig. 4. Device operation rotation diagram.

By utilizing encoder information, the specific rotation angle of the LiDAR probe relative to the stepper motor at each moment can be obtained. Let the rotation angle of the LiDAR with respect to the stepper motor be denoted as $\theta(t)$. The initial point cloud data P is then corrected to align its coordinate system with that of the stepper motor. The corrected point cloud data is represented as P', with the transformation given by $P' = R(\theta(t)) \cdot P$, where $R(\theta(t))$ is the rotation matrix based on the angle $\theta(t)$.

The corrected point cloud data is tightly integrated with inertial information. Pre-integration of the inertial data is performed to accumulate the sensor's motion trajectory. This pre-integration process primarily relies on the acceleration $a(t)$ and angular velocity $\omega(t)$ measured by the IMU to compute increments in position and orientation, as shown in Eq. (4).

$$\begin{cases} \Delta p = \int_{t_0}^{t_1} v(t) \cdot dt \\ \Delta v = \int_{t_0}^{t_1} a(t) \cdot dt \\ \Delta R = \int_{t_0}^{t_1} \omega(t) \cdot dt \end{cases} \tag{4}$$

The IMU-LiDAR fusion utilizes a Kalman filter, which includes a state vector representing position, velocity, quaternion, and the biases from the accelerometer and gyroscope. During the update process, the IMU performs predictions at a high frequency, while the LiDAR provides corrections at a lower frequency using feature residuals. Furthermore, bias compensation is implemented through online calibration via sliding window optimization.

Combining the point cloud constructed through the mobile scanning method with the corrected point cloud data and inertial data allows for real-time estimation of the sensor's 6DOF trajectory.

E. 3D Model Construction

The method for constructing a 3D model using LiDAR and IMU primarily consists of tightly coupled joint optimization of the LiDAR inertial odometry and point cloud mapping, as illustrated in Fig. 5.

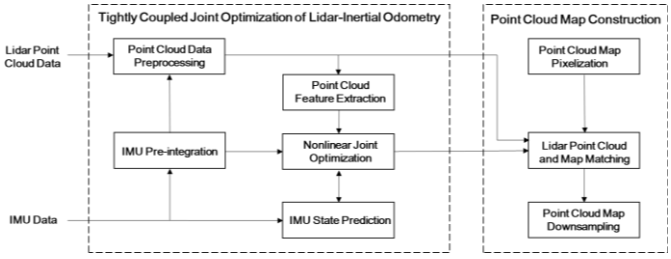

Fig. 5. System working principle.

In the tightly coupled joint optimization of the LiDAR inertial odometry, the IMU data is pre-integrated, and both intra-frame and inter-frame motions of the LiDAR are computed. The

calculated intra-frame motion is then used to preprocess the point cloud data, mitigating the effects of motion distortion through motion compensation using the IMU-derived trajectory. Additionally, ground segmentation is performed using RANSAC plane fitting with a defined inlier threshold, enabling the separation of ground points from other data. After this preprocessing, voxel downsampling is applied with differing resolutions for near-field and far-field regions to balance computational efficiency and detail retention. Feature extraction is then performed on the processed point cloud data, alongside IMU state prediction. Finally, based on the established IMU constraints and LiDAR constraints, a nonlinear optimization model is constructed to obtain the state variables required for the mapping process. The optimization process is supported by global techniques facilitated by the Ceres solver using the Levenberg-Marquardt algorithm, ensuring robust and accurate results.

In the point cloud mapping phase, the point cloud map is first voxelized. Subsequently, the optimized results from the odometry phase are used to match the LiDAR point cloud with the point cloud map. Lastly, the point cloud map undergoes downsampling to reduce its size.

IV. Engineering Applications

A. Project Background

The CMC project in the Democratic Republic of the Congo is a complex underground mining development system engineering project. The underground tunnel network includes multiple key areas and structures, with the areas to be scanned depicted in Fig. 6. These areas encompass light vehicle ramps, heavy vehicle ramps, and various sections such as the 1110, 940, and 990 levels, as well as the measures ramp. Additionally, the project involves significant underground facilities including ventilation shafts, auxiliary shafts, and water chambers.

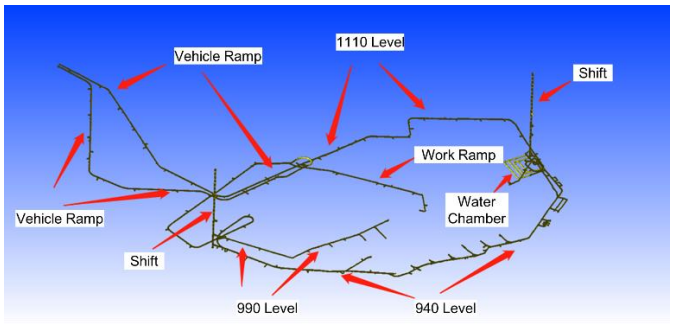

Fig. 6. Overall view of the underground mine survey area.

The geographical distribution and functional positioning of these tunnels and facilities result in a considerable project length, traversing various geological and structural layers. In such a complex underground environment, traditional measurement and modeling methods may not meet the required accuracy and efficiency standards. Therefore, a rapid tunnel modeling approach based on portable LiDAR technology is employed to achieve high-precision 3D positioning of the underground space.

B. Field Data Collection

Due to the complexity and long distances of the underground tunnel system, multiple data collection methods were employed to adapt to different environmental conditions and scenarios, as illustrated in Fig. 7. In accessible areas, operators conducted scanning with handheld devices. In the light and heavy vehicle ramp areas, scanning was performed from vehicles to enhance collection efficiency. In the 940 and 1110 level, where rainfall was prevalent, handheld scanning was utilized, with operators using umbrellas to shield against water spray, particularly in the 940 level. The device sensor continuously rotated at a steady speed to perform panoramic scanning, covering a distance of 100 meters, allowing for complete scanning with a single pass through the scene. For hazardous areas inaccessible to personnel, such as chutes and mined-out zones, drones or extension poles equipped with scanning devices were employed. These methods ensured high-quality data acquisition even in complex and dangerous environments.

Fig. 7. Handheld scanning and vehicle-mounted handheld scanning.

Data collection was conducted in segments due to the overall length of the underground tunnels. Each segment's data was distinguished by different colors, facilitating subsequent stitching and adjustments. To align the data with the geodetic coordinate system, the equipment needed to be calibrated to control points within the tunnels. In accessible areas, such as the tunnel floor, alignment was achieved by overlapping the crosshair on the device's base with the control point. In areas inaccessible to personnel, such as the tunnel ceiling, a visible laser on the device was used to aim at the control point. The positions of the control points were recorded on a mobile control device. This laser anchoring method did not require additional personnel, resulting in higher accuracy and allowing for single-person operation.

C. Indoor Data Processing

After data collection, the coordinates of the control points needed to be entered on the mobile control device. In the mobile control device's menu, the system for analysis was selected, and by clicking “Retrieve Data,” all collected data could be viewed. These data packets were named according to the collection time, with corresponding control point information displayed on the right side of each packet. By clicking on the control point information for a specific data packet, a window for inputting the control point coordinates would appear, where the geodetic coordinates (in meters) for the corresponding control point could be entered. After inputting the control point coordinates, the

relevant collected data was selected on the left side, followed by clicking the "Analyze" button to initiate data processing. The control point input interface on the mobile device is shown in Fig. 8.

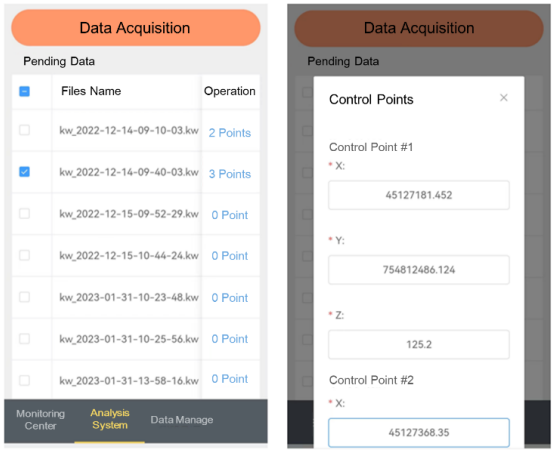

Fig. 8. Mobile interface for control point input.

After the data processing was completed, the data is transmitted to the PC via a network. The data folder contains several files, including filtermap.dxf, ControlPoint.txt, map.las, filter_map.las, map.pcd, filtermap.pcd, filtermap.ply, and Path.txt. Among these, filtermap.dxf contains the 3D model data generated automatically by the device, ControlPoint.txt records the geodetic and control point coordinates, while map.las and filter_map.las represent the original and decimated point cloud data of the map, respectively. Additionally, map.pcd and filtermap.pcd contain the original and decimated point cloud data in PCD format, filtermap.ply is the 3D object format point cloud data, and Path.txt contains the trajectory data of the device.

The LAS point cloud data undergoes filtering and denoising processes to eliminate noise generated by moving objects within the tunnel. This process retains valid points while reducing the overall data size to approximately one-tenth of the original. After filtering and denoising, a 3D model of the tunnel is created, generating a closed triangular mesh model that preserves the original morphology of the tunnel, as shown in Fig. 9.

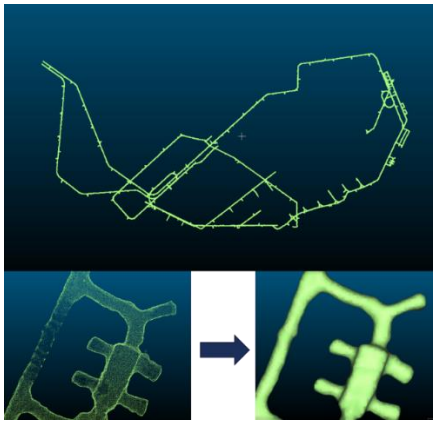

Fig. 9. Drift 3D model.

V. Results

A. Accuracy Validation

Once the tunnel's 3D model is established in point cloud processing software, it can be saved in DXF format and imported into 3D mining software such as Dimine for further processing. This facilitates a series of tasks related to geological surveying and mining operations, including ore body modeling, tunnel design, resource estimation, and extraction planning. By comparing the 3D model with the CAD base map in detail, the accuracy and completeness of the model can be analyzed, as shown in Fig. 10.

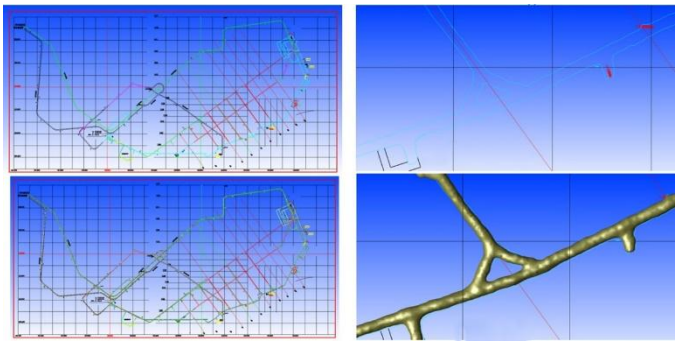

Fig. 10. Comparison of CAD drawing and model.

First, the CAD base map and the DXF format 3D model data are imported separately into the software. The comparison tool is then used to overlay the 3D model with the CAD base map to check their alignment. If discrepancies are identified between the 3D model and the CAD base map, adjustments and corrections can be made based on the comparison results to ensure high precision of the model.

The accuracy assessment involves comparing the 3D model with the actual tunnel, measuring deviations in both longitudinal and lateral positions. Several representative measurement points were selected at different locations within the tunnel, and actual measurements were taken. These data were then compared with the corresponding data in the 3D model, as shown in Table II.

TABLE II. Comparison between Measured Model and Actual Measurements

Measurement Point	*Measurement Content*	*Actual Value (m)*	*Measured Value (m)*	*Absolute Error (m)*	*Relative Error (%)*
Vehicle Ramp	Longitudinal Deviation	269.87	270.12	-0.25	0.09
	Lateral Deviation	4.72	4.74	-0.02	0.42
Water Chamber	Longitudinal Deviation	15.18	15.14	0.04	0.26
	Lateral Deviation	4.21	4.22	-0.01	0.24
Stope Substation	Longitudinal Deviation	5.37	5.36	0.01	0.19
	Lateral Deviation	4.92	4.93	-0.01	0.20

The results demonstrate that the absolute errors across all test points were minimal, with relative errors ranging from 0.09% to 0.42%, ensuring that the generated 3D models meet precision requirements for mining applications. These findings indicate the reliability of the presented method in achieving high-accuracy 3D modeling in complex underground environments.

Beyond validation through direct measurements, 3D models were also compared against original design CAD drawings within mining software (e.g., DIMINE). The overlay alignment evaluation revealed minimal discrepancies, confirming the completeness and consistency of the 3D models with the engineering designs (Fig. 10). This validation process underscores the potential of the proposed method for enhancing tunnel design implementation and quality control.

B. Efficiency Analysis

The efficiency of the proposed method was assessed by examining the time required for data collection and processing compared to traditional methods such as total station measurements and static LiDAR scanning. The portable LiDAR system significantly reduced fieldwork times due to its ability to capture spatial data continuously and autonomously while in motion. Specifically, the system completed a 2.3 km tunnel network survey in approximately 6 hours, including setup, scanning, and preliminary control point calibration. Traditional methods would typically require at least 2–3 days for similar coverage, highlighting the advantages of the portable LiDAR solution in terms of operational efficiency.

Furthermore, the automated data processing workflow reduced the time needed for point cloud filtering, denoising, and stitching by at least 30% compared to conventional software pipelines. The integration of SLAM and IMU technologies eliminated the dependency on fixed reference points, further streamlining data collection in environments with limited access or visibility.

C. Safety and Adaptability

The adaptability and safety of the proposed method were demonstrated through its successful deployment in hazardous and challenging underground environments. The compact and portable design of the scanning device facilitated access to narrow and confined spaces, eliminating the need for extensive manual setups. Additionally, automated scanning from mobile platforms (e.g., vehicles) or remote systems (e.g., drones) allowed for data collection in areas that were otherwise inaccessible or unsafe for personnel, such as waterlogged tunnels and mined-out zones.

The flexibility of the system was further underscored by its performance in varying environmental conditions. For instance, handheld scanning with umbrellas in the 940 level ensured high-quality data acquisition despite water spray and poor lighting. These capabilities emphasize the robustness of the system in adapting to diverse underground scenarios.

D. Discussion

The proposed portable LiDAR-based rapid modeling method demonstrates significant advancements in accuracy, efficiency, and adaptability for underground mining applications. The integration of SLAM and IMU technologies effectively addresses common challenges in GPS-denied environments, ensuring reliable data collection and high-resolution 3D modeling. Compared to traditional surveying methods, the proposed approach achieves superior time efficiency and operational flexibility while maintaining precision, as evidenced by relative errors below 0.5% and successful deployment in complex tunnel networks. Furthermore, the system's portability and ability to operate under adverse conditions, such as low light, dust, and water spray, highlight its robustness and practical value for diverse underground scenarios.

Despite these advantages, residual challenges remain. Pose error accumulation during extended operations and computational demands for large-scale point cloud processing represent areas for improvement. Environmental factors, such as extreme humidity or dust, may also introduce noise, impacting data quality. Future research should focus on optimizing SLAM algorithms, developing real-time processing capabilities, and integrating complementary sensors to enhance system performance. Additionally, further miniaturization and automation could expand its applications across other industries.

Overall, this study provides a comprehensive solution for efficient and accurate tunnel modeling, addressing critical limitations of traditional methods and laying a foundation for broader adoption of portable LiDAR technologies in mining and beyond.

VI. Conclusion

This study addresses the challenge of rapid 3D modeling of underground mining tunnels by proposing an innovative solution based on portable 3D laser scanning technology and SLAM techniques. Experimental validation demonstrates the feasibility and effectiveness of this approach in complex environments. By integrating portable 3D laser scanning technology with SLAM algorithms and IMU, this research successfully achieves efficient 3D modeling of underground tunnels without relying on external positioning signals. This method effectively overcomes the limitations of traditional measurement techniques, such as low efficiency and restricted accuracy in underground settings, significantly enhancing data collection speed and quality while providing technical support for high-resolution modeling of complex tunnel networks. The findings indicate that portable devices can maintain measurement stability and precision even in adverse underground conditions characterized by poor lighting and air quality, offering new insights for 3D modeling in other complex subterranean environments. The generated 3D models meet practical engineering requirements in terms of accuracy, completeness, and visualization, making them applicable in various domains, including geological surveying, engineering design, construction acceptance, and safety management. Moreover, this study demonstrates the flexibility and practicality of the technology in complex scenarios, highlighting its ease of operation and high degree of automation in data processing, thus providing crucial technical support for digital mining and intelligent mine management.

However, this research has certain limitations, and future studies will focus on optimizing SLAM algorithms to reduce pose error accumulation, as well as integrating multi-sensor

fusion technologies (e.g., collaborative use of vision and LiDAR) to enhance data collection accuracy. Building on this foundation, the development of more compact and efficient portable devices to meet the surveying needs of various complex environments will be pursued.

ACKNOWLEDGMENT

This research was supported by the Key Research and Development Program of Hunan Province (Grant No: 2022GK2061).

REFERENCES

[1] S. Tavani et al., "Smartphone assisted fieldwork: Towards the digital transition of geoscience fieldwork using LiDAR-equipped iPhones," Earth-Science Reviews, vol. 227, p. 103969, Apr. 2022, doi: 10.1016/j.earscirev.2022.103969.

[2] T. G. Garrison et al., "Assessing the lidar revolution in the Maya lowlands: A geographic approach to understanding feature classification accuracy," Progress in Physical Geography: Earth and Environment, vol. 47, no. 2, pp. 270–292, Apr. 2023, doi: 10.1177/03091333221138050.

[3] P. Padmanabhan, C. Zhang, and E. Charbon, "Modeling and Analysis of a Direct Time-of-Flight Sensor Architecture for LiDAR Applications," Sensors, vol. 19, no. 24, Art. no. 24, Jan. 2019, doi: 10.3390/s19245464.

[4] L. Zhao, M. Zhang, and X. Jin, "Construction and application of a high precision 3D simulation model for geomechanics of the complex coal seam," Sci Rep, vol. 11, no. 1, p. 21374, Nov. 2021, doi: 10.1038/s41598-021-00709-5.

[5] L. Chen et al., "High-Precision Positioning, Perception and Safe Navigation for Automated Heavy-Duty Mining Trucks," IEEE Transactions on Intelligent Vehicles, vol. 9, no. 4, pp. 4644–4656, Apr. 2024, doi: 10.1109/TIV.2024.3375273.

[6] M. Laguillo, P. Segarra, J. A. Sanchidrián, and F. Beitia, "A novel borehole surveying system for underground mining: Design and performance assessment," Measurement, vol. 194, p. 111021, May 2022, doi: 10.1016/j.measurement.2022.111021.

[7] S. Kahraman, J. Rostami, and A. Naeimipour, "Review of Ground Characterization by Using Instrumented Drills for Underground Mining and Construction," Rock Mech Rock Eng, vol. 49, no. 2, pp. 585–602, Feb. 2016, doi: 10.1007/s00603-015-0756-4.

[8] A. Aryan, F. Bosché, and P. Tang, "Planning for terrestrial laser scanning in construction: A review," Automation in Construction, vol. 125, p. 103551, May 2021, doi: 10.1016/j.autcon.2021.103551.

[9] C. Wu, Y. Yuan, Y. Tang, and B. Tian, "Application of Terrestrial Laser Scanning (TLS) in the Architecture, Engineering and Construction (AEC) Industry," Sensors, vol. 22, no. 1, Art. no. 1, Jan. 2022, doi: 10.3390/s22010265.

[10] A. Piekarczuk, A. Mazurek, J. Szer, and I. Szer, "A Case Study of 3D Scanning Techniques in Civil Engineering Using the Terrestrial Laser Scanning Technique," Buildings, vol. 14, no. 12, Art. no. 12, Dec. 2024, doi: 10.3390/buildings14123703.

[11] S. Kumar Singh, B. Pratap Banerjee, and S. Raval, "A review of laser scanning for geological and geotechnical applications in underground mining," International Journal of Mining Science and Technology, vol. 33, no. 2, pp. 133–154, Feb. 2023, doi: 10.1016/j.ijmst.2022.09.022.

[12] R. Hudson, F. Faraj, and G. Fotopoulos, "Review of close-range three-dimensional laser scanning of geological hand samples," Earth-Science Reviews, vol. 210, p. 103321, Nov. 2020, doi: 10.1016/j.earscirev.2020.103321.

[13] J. Telling, A. Lyda, P. Hartzell, and C. Glennie, "Review of Earth science research using terrestrial laser scanning," Earth-Science Reviews, vol. 169, pp. 35–68, Jun. 2017, doi: 10.1016/j.earscirev.2017.04.007.

[14] J. Li et al., "Real-time self-driving car navigation and obstacle avoidance using mobile 3D laser scanner and GNSS," Multimed Tools Appl, vol. 76, no. 21, pp. 23017–23039, Nov. 2017, doi: 10.1007/s11042-016-4211-7.

[15] X. Lian et al., "Biomass Calculations of Individual Trees Based on Unmanned Aerial Vehicle Multispectral Imagery and Laser Scanning Combined with Terrestrial Laser Scanning in Complex Stands," Remote Sensing, vol. 14, no. 19, Art. no. 19, Jan. 2022, doi: 10.3390/rs14194715.

[16] M. J. Sumnall et al., "Effect of varied unmanned aerial vehicle laser scanning pulse density on accurately quantifying forest structure," International Journal of Remote Sensing, vol. 43, no. 2, pp. 721–750, Jan. 2022, doi: 10.1080/01431161.2021.2023229.

[17] C. Zhang, "Mine laneway 3D reconstruction based on photogrammetry," Transactions of Nonferrous Metals Society of China, vol. 21, pp. s686–s691, Dec. 2011, doi: 10.1016/S1003-6326(12)61663-X.

[18] A. Adamek, J. Będkowski, P. Kamiński, R. Pasek, M. Pełka, and J. Zawiślak, "Method for Underground Mining Shaft Sensor Data Collection," Sensors, vol. 24, no. 13, Art. no. 13, Jan. 2024, doi: 10.3390/s24134119.

[19] X. Lian and H. Hu, "Terrestrial laser scanning monitoring and spatial analysis of ground disaster in Gaoyang coal mine in Shanxi, China: a technical note," Environ Earth Sci, vol. 76, no. 7, p. 287, Apr. 2017, doi: 10.1007/s12665-017-6609-6.

[20] L. Fahle, E. A. Holley, G. Walton, A. J. Petruska, and J. F. Brune, "Analysis of SLAM-Based Lidar Data Quality Metrics for Geotechnical Underground Monitoring," Mining, Metallurgy & Exploration, vol. 39, no. 5, pp. 1939–1960, Oct. 2022, doi: 10.1007/s42461-022-00664-3.

[21] Z. Ren, L. Wang, and L. Bi, "Robust GICP-Based 3D LiDAR SLAM for Underground Mining Environment," Sensors, vol. 19, no. 13, Art. no. 13, Jan. 2019, doi: 10.3390/s19132915.

[22] A. Ellmann, K. Kütimets, S. Varbla, E. Väli, and S. Kanter, "Advancements in underground mine surveys by using SLAM-enabled handheld laser scanners," Survey Review, vol. 54, no. 385, pp. 363–374, Jul. 2022, doi: 10.1080/00396265.2021.1944545.

[23] L. Wang, S. Zhang, J. Qi, H. Chen, and R. Yuan, "Research on IMU-Assisted UWB-Based Positioning Algorithm in Underground Coal Mines," Micromachines, vol. 14, no. 7, Art. no. 7, Jul. 2023, doi: 10.3390/mi14071481.

[24] M.-G. Li, H. Zhu, S.-Z. You, and C.-Q. Tang, "UWB-Based Localization System Aided With Inertial Sensor for Underground Coal Mine Applications," IEEE Sensors Journal, vol. 20, no. 12, pp. 6652–6669, Jun. 2020, doi: 10.1109/JSEN.2020.2976097.

[25] S. Tong, Q. Jia, N. Song, W. Zhou, T. Duan, and C. Bao, "Determination of gold(III) and palladium(II) in mine samples by cloud point extraction preconcentration coupled with flame atomic absorption spectrometry," Microchim Acta, vol. 172, no. 1, pp. 95–102, Feb. 2011, doi: 10.1007/s00604-010-0466-2.

[26] Y. Wang, W. Tu, and H. Li, "Fragmentation calculation method for blast muck piles in open-pit copper mines based on three-dimensional laser point cloud data," International Journal of Applied Earth Observation and Geoinformation, vol. 100, p. 102338, Aug. 2021, doi: 10.1016/j.jag.2021.102338.

[27] S.-J. Lee and S.-O. Choi, "Analyzing the Stability of Underground Mines Using 3D Point Cloud Data and Discontinuum Numerical Analysis," Sustainability, vol. 11, no. 4, Art. no. 4, Jan. 2019, doi: 10.3390/su11040945.

[28] M. Chen, Y. Feng, S. Wang, and Q. Liang, "A Mine Intersection Recognition Method Based on Geometric Invariant Point Detection Using 3D Point Cloud," IEEE Robotics and Automation Letters, vol. 7, no. 4, pp. 11934–11941, Oct. 2022, doi: 10.1109/LRA.2022.3208366.